**A genomic integration platform for heterologous cargo encapsulation in 1,2-propanediol utilization bacterial microcompartments**

Taylor M. Nichols [a], Nolan W. Kennedy [b], Danielle Tullman-Ercek [a, c, d]

[a] Department of Chemical and Biological Engineering, Northwestern University, 2145 Sheridan Road, Technological Institute E136, Evanston, IL, 60208, USA

[b] Interdisciplinary Biological Sciences Graduate Program, Northwestern University, 2205 Tech Drive, 2-100 Hogan Hall, Evanston, IL, 60208, USA

[c] Center for Synthetic Biology, Northwestern University, 2145 Sheridan Road, Technological Institute B486, Evanston, IL, 60208, USA

[d] Corresponding Author: ercek@northwestern.edu

Declarations of interest: none

**Abstract**

Bacterial microcompartments (MCPs) are protein structures that encapsulate specific metabolic pathways in bacteria. The 1,2-propanediol utilization (Pdu) MCP in *Salmonella enterica* serovar Typhimurium LT2 encapsulates the pathway for 1,2-propanediol degradation to sequester a toxic intermediate, enable cofactor recycling, and enhance pathway flux. The Pdu MCP has potential as an enclosed scaffold for metabolic engineering applications. To successfully use Pdu MCPs for this purpose, however, methods to enable and control heterologous cargo encapsulation are critical. To this end, we here developed a genomic expression platform for cargo encapsulation in Pdu MCPs. We integrated signal sequence-tagged fluorescent reporters into the *pdu* operon in place of native Pdu enzymes and evaluated the resulting expression and encapsulation levels. We found that fluorescent reporters were successfully co-encapsulated, with varying relative encapsulation levels achieved when using different integration locus and signal sequence combinations. We also observed that the native Pdu signal sequences mediated different encapsulation efficiencies independent of expression levels. This work establishes the genomic integration platform as a viable method for controlling cargo encapsulation, expanding the toolkit toward engineering the Pdu MCP as a tunable nanobioreactor.

**Keywords**

Bacterial microcompartments; *Salmonella*; genomic integration; cargo encapsulation; metabolic engineering; Pdu

## 1 Introduction

Metabolic engineering is a promising platform for the sustainable production of chemicals, drugs, and biofuels in living cells. However, the efficient use of heterologous pathways in different host organisms can be impeded by toxic or reactive intermediates, off-target interactions, cofactor imbalances, and resource competition. To mitigate these issues, different scaffold systems can be used to colocalize and organize heterologous pathway components [1–7]. However, computational evidence suggests that pathway flux could be further enhanced for certain pathways using compartmentalization [8–10]. To this end, bacterial microcompartments have potential as enclosed scaffolds for metabolic engineering applications (Fig. 1A).

Bacterial microcompartments (MCPs) are protein structures that are found in approximately 66% of bacterial phyla and function to encapsulate the components required for specific metabolic processes [11,12]. The 1,2-propanediol utilization (Pdu) MCP (Fig. 1A) forms natively in *Salmonella enterica* serovar Typhimurium LT2 to efficiently metabolize 1,2-propanediol (1,2-PD) [13]. The primary metabolic pathway to propionate includes the diol dehydratase PduCDE, propionaldehyde dehydrogenase PduP, phosphotransacylase PduL, and propionate kinase PduW [14–18]. Notably, the toxic intermediate propionaldehyde is formed within the Pdu MCP in the first pathway step by PduCDE. The protein shell of the Pdu MCP acts as a selectively permeable barrier, functioning primarily to sequester propionaldehyde and mitigate its toxicity [19–22]. Sequestration also serves to enhance pathway flux by increasing the local concentration of propionaldehyde within the Pdu MCP [23]. The encapsulated propionaldehyde intermediate can subsequently be converted by two different enzymes in a coupled reaction within the Pdu MCP (Fig. 1A). Specifically, through the primary pathway propionaldehyde is converted by PduP in a reaction that requires NAD+ and generates NADH, and alternatively is converted by the 1-propanol dehydrogenase PduQ in a reaction that utilizes NADH and generates NAD+ [16,24]. The regeneration of NAD+/NADH between these two

reactions provides one example of internal cofactor recycling through which the Pdu MCP creates putative private cofactor pools for the encapsulated pathway enzymes [24–26].

Heterologous enzymes and pathways can be successfully encapsulated within Pdu MCPs [27–29]. Notably, Lawrence and colleagues developed an ethanol nanobioreactor by directing two enzymes to the Pdu MCP lumen which convert pyruvate to ethanol [28]. Encapsulation within the Pdu MCP is enabled by signal sequences comprising the N-terminal 18-20 amino acids of the Pdu enzymes PduD, PduL, and PduP, which can mediate the encapsulation of both the native enzymes and tagged heterologous cargo [25,30,31]. Non-native signal sequences, *de novo* signal sequences, and *de novo* protein interactions also mediate encapsulation within Pdu MCPs, and cargo loading levels can be controlled using different expression levels, signal sequence combinations, and induction conditions [29,32–34]. However, efforts to date largely rely on plasmid-based expression systems, which we expect will become more difficult to implement with more complex metabolic pathways and at larger scales.

Genomic expression systems are increasingly practical alternatives to plasmid-based expression systems for metabolic engineering applications. Genomic integration can enable more stable and consistent cargo expression while eliminating the use of antibiotics or other means of selection [35–37]. In this paper we demonstrate a platform for heterologous cargo encapsulation in Pdu MCPs using a genomic expression system. The *pdu* operon encodes the native shell proteins and Pdu enzymes comprising the Pdu MCP, with expression induced by 1,2-PD and the transcriptional regulator PocR [13,38–40]. Here, we integrated different fluorescent reporters tagged with native Pdu signal sequences into the *pdu* operon in place of native Pdu enzymes (Fig. 1B). We then assessed strains and purified MCPs to characterize the cargo expression and encapsulation levels resulting from different integration locus and signal sequence combinations. From this analysis we determined *pdu* operon loci that are permissible to integrations and established general guidelines for parameter selection when using this genomic cargo expression system. This work expands the toolkit for controlling encapsulation of

heterologous cargo within Pdu MCPs, further enabling its use as a tunable engineered nanobioreactor.

## 2 Materials and Methods

### *2.1 Strains, Media, and Growth Conditions*

Strains used in this study include *Salmonella enterica* serovar Typhimurium LT2 and *Escherichia coli* DH10B (Table 1). All *S. enterica* LT2 strains with genomic integrations were generated via recombineering [41,42]. Briefly, the *cat/sacB* selection cassette was amplified from the TUC01 genome and fluorescent reporter constructs were amplified from their respective plasmids (Table 2) using primers with added homology to the different integration loci (Tables S1, S4). We used an optimized variant of green fluorescent protein, mut2, denoted GFP in this work [44] and mCherry for red fluorescent protein [45]. For each locus, the corresponding *cat/sacB* cassette was then integrated into the genome, replacing the native gene. Different fluorescent reporters were subsequently integrated at these same loci, replacing the *cat/sacB* cassette. For each resulting strain, the modified locus of interest was amplified from the genome to confirm the intended integration via Sanger sequencing.

*S. enterica* LT2 strains were grown as previously described [46]. Briefly, single colonies were picked from agar plates and grown in 5 mL Lysogeny Broth, Miller (LB-Miller) for 24 hours at 30°C, 225 RPM. These were subcultured 1:1000 into No Carbon-E (NCE) minimal media (29 mM potassium phosphate monobasic, 34 mM potassium phosphate dibasic, 17 mM sodium ammonium hydrogen phosphate), supplemented with 1 mM magnesium sulfate, 50 µM ferric citrate, and 42 mM succinate. Unless otherwise indicated, NCE media also was supplemented with 55 mM 1,2-PD to induce MCP formation; 1,2-PD also induced cargo expression for the genomic integration strains. NCE cultures were grown at 37°C, 225 RPM. Antibiotics were added to LB cultures (34 µg/mL chloramphenicol or 50 µg/mL kanamycin) and NCE cultures (17 µg/mL chloramphenicol), as necessary.

### *2.2 Plasmid Construction*

Signal sequences were modified or added to fluorescent reporter constructs via PCR amplification using primers with overhangs containing the appropriate sequences (Tables S1, S3). These were then cloned into arabinose-inducible (pBAD) or tetracycline-inducible (pTET) plasmids (Table 2) using Golden Gate cloning with the type IIS restriction enzyme BsaI [47]. *E. coli* DH10B was transformed with the resulting plasmids and plasmid sequences were confirmed via Sanger sequencing. Wild type *S. enterica* LT2 was transformed with the sequence-confirmed plasmids.

### *2.3 Flow Cytometry*

Relative encapsulation levels for plasmid-based cargo expressed in *S. enterica* LT2 were evaluated using the flow cytometry assay previously described [43,46]. Briefly, NCE cultures both with and without 1,2-PD were grown as described in Section 2.1 using culture volumes of 5 mL in 24-well blocks. When the culture $OD_{600}$ reached ~0.4, samples were induced with 0.02% (w/v) arabinose and grown for an additional 5 hours at 37°C, 225 RPM. Samples were diluted to a target $OD_{600}$ of ~0.01-0.04 in 200 µL of phosphate buffered saline with 2 g/L kanamycin in 96-well plates. Events were collected for each sample using the Attune NxT Acoustic Focusing flow cytometer equipped with blue and green lasers, and analysis carried out using FlowJo software. Events were gated using the forward and side scatter channels to distinguish cells from debris, and average fluorescence was calculated using the geometric mean.

### *2.4 MCP Purification*

For MCP purification, NCE cultures were grown as described in Section 2.1 using culture volumes of 200 mL in 1 L flasks. Reserve samples of culture were taken as necessary for fluorescence microscopy and western blotting, and the remaining culture was harvested and lysed. MCPs were purified from the lysate through a centrifugation process as previously described [32,46,48]. Briefly, lysate was centrifuged at 12,000xg to pellet cell debris, and the

resulting supernatant subsequently was centrifuged at 21,000xg to pellet MCPs. The MCP pellet was collected and stored at 4°C until use. The protein concentration of each purified MCP sample was measured using the Pierce™ BCA Protein Assay Kit (Thermo Scientific).

### *2.5 Fluorescence Microscopy*

For strains expressing fluorescent reporters, fluorescence microscopy was used to visualize and evaluate cargo encapsulation. Cells were viewed using a Nikon Eclipse Ni-U upright microscope with a 100X oil immersion objective, and images captured using an Andor Clara digital camera and Nikon NIS Elements software. GFP fluorescence images were collected using a C-FL Endow GFP HYQ bandpass filter and mCherry fluorescence images were collected using a C-FL Y-2E/C filter. GFP fluorescence images were taken with 200 ms exposure and mCherry fluorescence images were taken with 400 ms exposure. Unless otherwise noted, all images within the same data set were adjusted identically for brightness and contrast using ImageJ software [49].

### *2.6 SDS-PAGE and Western Blotting*

Purified MCP and whole cell lysate (WCL) samples were separated on 15% SDS-PAGE gels. Loading for MCP samples initially was normalized by protein concentration as measured by BCA, and then adjusted by densitometry as needed to correct for potential contaminants within the samples. Loading for WCL samples was normalized by the culture $OD_{600}$ at the time of harvest. Protein gels were subsequently stained by Coomassie or transferred to PVDF membranes for western blotting as previously described [46].

For western blotting, membranes were incubated in a 1:2000 dilution of mouse anti-GFP (Clontech) or rat anti-mCherry (Thermo Fisher Scientific) primary antibody in TBST (20 mM Tris, 150 mM NaCl, pH 7.5 with 0.05% Tween 20) with 1% (w/v) dry milk. These were subsequently incubated in a 1:1000 dilution of HRP-conjugated goat anti-mouse or a 1:5000 dilution of HRP-conjugated goat anti-rat secondary antibody (Thermo Fisher Scientific) in TBST. Blots were

developed and imaged using chemiluminescent substrates (Thermo Scientific SuperSignal™ West Pico PLUS or Femto) and the Bio-Rad ChemiDoc XRS+ imaging system. Densitometry analysis was performed using Bio-Rad Image Lab Software. For MCPs, the densitometry results from western blots were normalized using the PduB' band on the corresponding Coomassie-stained protein gels.

### *2.7 Negative Stain Transmission Electron Microscopy*

Samples of purified MCPs were set onto 400 mesh Formvar-coated copper grids after treatment with glow discharge (PELCO easiGlow). A volume of 10 µL of MCPs at a concentration of 100-200 µg/mL were set on the grids for 2 minutes. The grids were washed with water and treated with 10 µL of 2% (v/v) glutaraldehyde for 2 minutes. Then the samples were washed again with water and stained with 10 µL of 1% (w/v) uranyl acetate for 2 minutes. The samples were dried and stored at room temperature until imaging. Images were collected at the Electron Probe Instrumentation Center (EPIC) at Northwestern University using the Hitachi HT-7700 Biological S/TEM Microscope and the Galtan Orius 4k x 2.67k digital camera.

## 3 Results and Discussion

### *3.1 Construction of genomic integration strains for GFP expression and encapsulation*

For the genomic integration platform, we first constructed strains of *S. enterica* LT2 with different GFP reporters integrated at different *pdu* operon loci (Fig. 1B, Table 1). Specifically, we integrated GFP tagged with the native N-terminal signal sequences $PduD^{1-20}$ (ssPduD), $PduL^{1-20}$ (ssPduL), or $PduP^{1-18}$ (ssPduP), as well as untagged GFP, into the *pdu* operon at the *pduD*, *pduL*, *pduP*, or *pduQ* locus. Notably, there is a coding sequence overlap between *pduP* and the upstream gene *pduO*. Recognizing that the integration of cargo tagged with ssPduD or ssPduL at the *pduP* locus would result in the disruption of the *pduO* stop codon, we instead used signal sequence variants designed to maintain the native *pduO* coding sequence (Table S2).

Specifically, for ssPduD we replaced the glutamic acid at residue 2 with serine, resulting in the variant ssPduD(E2S).

To compare the ssPduD(E2S) variant with the native signal sequences, we evaluated cargo encapsulation levels using a flow cytometry assay previously established for plasmid-based expression systems [43]. Briefly, we append signal sequence-GFP reporters with a SsrA degradation tag [50,51], resulting in the degradation of unencapsulated cargo. Flow cytometry measurements then indicate levels of encapsulated cargo only. For this study, the reporter fusions ssPduD-GFPmut2-ssrA, ssPduD(E2S)-GFPmut2-ssrA, ssPduL-GFPmut2-ssrA, and ssPduP-GFPmut2-ssrA were expressed from pBAD plasmids in *S. enterica* LT2 grown both with and without 1,2-PD. Our prior work demonstrates that the ratio of GFP fluorescence for these two conditions, as measured by flow cytometry, provides the most accurate representation of relative encapsulation levels [43]. This analysis for the evaluated signal sequence-GFP reporters showed that the encapsulation of GFP mediated by ssPduD(E2S) was comparable to that mediated by native ssPduD (Fig. S1). As a result, ssPduD(E2S) was used in place of ssPduD for cargo integrations at the *pduP* locus. A similar variant for ssPduL was also designed but did not mediate encapsulation when evaluated so was not included in this study.

### *3.2 Encapsulation levels are independent from expression levels for genomically encoded cargo*

To evaluate the encapsulation behaviors of genomically encoded cargo, we visualized strains with GFP reporters integrated at each locus using fluorescence microscopy. Encapsulation of fluorescent cargo within Pdu MCPs is indicated by the presence of fluorescent puncta within the cell, whereas unencapsulated cargo is observed as diffuse fluorescence. We first examined strains with integrations at the *pduD* locus. Fluorescent puncta were present for LT2 *ΔpduD::ssPduD-gfpmut2*, LT2 *ΔpduD::ssPduL-gfpmut2*, and LT2 *ΔpduD::ssPduP-gfpmut2,* while only diffuse fluorescence was observed for *ΔpduD::gfpmut2* (Fig. 2A). Unexpectedly, we

also noted varying levels of encapsulated and diffuse GFP within cells for the strains with fluorescent puncta. Notably, we observed minimal diffuse GFP for LT2 *ΔpduD::ssPduD-gfpmut2*, and we saw mostly diffuse GFP for LT2 *ΔpduD::ssPduL-gfpmut2* with few puncta.

To further evaluate the observed encapsulation behaviors, we purified MCPs from each of the *pduD* locus integration strains. The purified MCPs were evaluated for morphology and composition by transmission electron microscopy (TEM) and SDS-PAGE, respectively. Each strain formed intact MCPs with morphology comparable to MCPs purified from wild-type *S. enterica* LT2 (LT2 WT) when compared using TEM (Fig. 2A). When separated on SDS-PAGE gels and stained, the purified MCPs also exhibited the typical MCP banding pattern except that we did not see bands for PduD and the associated enzyme subunits PduC and PduE (Fig. 2B). This result was expected for integrations at the *pduD* locus because PduD is also responsible for recruiting PduC and PduE into the Pdu MCP [31]. To assess cargo encapsulation levels, we evaluated the purified MCP samples by western blotting against GFP. Similarly, to assess cargo expression levels, we evaluated whole cell lysate (WCL) samples from each strain by western blotting against GFP. The resulting densitometry analyses revealed that relative cargo encapsulation levels varied for each strain, consistent with the fluorescence microscopy results (Fig. 2B,C). However, relative cargo expression levels were consistent for each strain, with no statistically significant differences found (single factor ANOVA, $p=0.120$) (Fig. 2B,D). The variation in cargo encapsulation levels is therefore not explained by the variation in cargo expression levels.

To determine if the encapsulation and expression trends were consistent for integrations at different operon loci, we also carried out western blotting of purified MCPs and WCL from strains with GFP reporters integrated at the *pduL*, *pduP*, and *pduQ* loci. The αGFP western blots and resulting densitometry analyses showed that for both the *pduL* and *pduQ* locus integration strains, the relative cargo encapsulation levels varied, while the cargo expression levels remained consistent (Fig. 3, Fig. S2). Further, for the *pduD, pduL,* and *pduQ* locus

integration strains, generally ssPduD-GFPmut2 has the highest relative encapsulation level, followed by ssPduP-GFPmut2, and then ssPduL-GFPmut2 with the lowest relative encapsulation level (when detected above background) (Fig. 2C, 3A). Note that while these trends were consistent for each replicate blot, they were not all significant (i.e., p-value not always <0.05) when comparing across replicates, likely due to the variation inherent to western blotting (Fig. 2C, 3A). For the *pduP* locus integration strains a comparable trend was not observed. Instead, ssPduD(E2S)-GFPmut2 and ssPduP-GFPmut2 had similar encapsulation levels (Fig. 3A, Fig. S2).

For the *pduD, pduL,* and *pduQ* locus integration strains, no strong correlation is observed between the relative encapsulation levels and relative expression levels of the different GFP reporters (Fig. S3). This supports the observation that encapsulation levels are independent from expression levels at each of these loci. Taken collectively, these results indicate that the native Pdu signal sequences mediate different encapsulation efficiencies, with ssPduD>ssPduP>ssPduL. It is possible that a similar trend in encapsulation efficiency exists for the *pduP* locus integration strains, with the expected encapsulation levels of ssPduD(E2S)-GFPmut2 and ssPduP-GFPmut2 impacted by genomic context or potential differences in expression, though no statistically significant difference between the cargo expression levels was noted.

### *3.3 A range of encapsulation levels can be attained by selecting different integration locus and signal sequence combinations*

When comparing all genomic integrations strains, we observed that cargo expression levels varied across loci, even while largely consistent within a specific locus (Fig. 2B,D, Fig. 3B, Fig. S2). We also observed that the encapsulation levels of specific signal sequence-GFP reporters varied when expressed from different loci (Fig. 2B,C, Fig. 3A, Fig. S2). These results indicate that both the signal sequence and integration locus used can impact the level of cargo

encapsulation within Pdu MCPs. Notably, by using different integration locus and signal sequence combinations, we were able to attain a range of cargo encapsulation levels. These results provide a general framework for use of this genomic integration platform, specifically for selecting integration loci and signal sequences for heterologous cargo, with the ability to select for various relative encapsulation levels.

### *3.4 Integrations at the pduL locus result in aberrant cell and MCP phenotypes*

As with the *pduD* locus integration strains, we visualized the *pduL*, *pduP*, and *pduQ* locus integration strains by fluorescence microscopy, and assessed purified MCPs from each strain for morphology and composition. For the *pduP* and *pduQ* locus integration strains, we observed cells of typical morphology with punctate and diffuse fluorescence as expected for the different signal sequence-GFP reporters (Fig. S4). Purified MCPs from each strain also had typical morphology, and when separated by SDS-PAGE and stained, showed MCP banding patterns consistent with the enzyme knockouts (Fig. S2, Fig. S4). For strains with integrations at the *pduL* locus, however, aberrant phenotypes were present (Fig. 4). Specifically, when each of these strains were grown in the presence of 1,2-PD, we observed linked cells by phase and fluorescence microscopy. We also discerned large areas of punctate fluorescence, which suggested cargo aggregation, MCP aggregation, or MCPs of aberrant size. Upon evaluating the structures purified from these strains by TEM, we indeed found enlarged and elongated structures resembling rods and cones, with some MCPs of typical morphology.

It is likely that these aberrant cells and protein structures form because *pduL* is located directly upstream of shell and structural proteins on the *pdu* operon (Fig. 1B). Integrations at this locus may therefore cause polar effects that disrupt the expression of downstream operon components, particularly of the shell protein PduN. PduN forms the vertices of the Pdu MCP shell, and MCPs with aberrant morphologies, including elongated structures, were observed for a *ΔpduN* mutant of *S. enterica* LT2 [52]. While signal sequence-GFP reporters do target these

protein structures in the *pduL* locus integration strains, it is unclear what impact the altered morphology will have on desired function; additional characterization of these structures is warranted but beyond the scope of this work.

### *3.5 Co-encapsulation of multiple genomically encoded cargo can be attained with varying relative encapsulation levels*

To further demonstrate the feasibility of the genomic integration platform for metabolic engineering applications, we aimed to co-encapsulate multiple genomically encoded cargo within Pdu MCPs. Our lab previously demonstrated the colocalization of GFP and mCherry reporters to Pdu MCPs in *S. enterica* LT2 using a plasmid-based expression system [32]. We therefore generated four strains with signal sequence-GFP reporter fusions integrated at the *pduD* or *pduP* locus and signal sequence-mCherry reporter fusions integrated at the second locus (Fig. 5A, Table 1). For each strain, one of the reporters was tagged with ssPduD while the other reporter was tagged with ssPduP, with the variant ssPduD(E2S) again used for integrations at the *pduP* locus. We also generated strains with only the mCherry reporters integrated into the *pdu* operon, corresponding to the integration locus and signal sequence combinations used for the dual integration strains (Table 1).

We first visualized the dual integration strains by fluorescence microscopy. For each strain, we observed fluorescent puncta in both the GFP fluorescence images and mCherry fluorescence images, with encapsulation behaviors as expected for the signal sequences used with each reporter (Fig. 5B). We also noted that the puncta were consistent across both fluorescence images, suggesting colocalization of the tagged fluorescent cargo to Pdu MCPs. To further evaluate the observed encapsulation behaviors, we purified and assessed MCPs from each of the dual integration strains. Results from TEM indicated that each strain formed intact MCPs with morphology comparable to MCPs purified from LT2 WT (Fig. 5B). We then performed western blotting of these purified MCP samples against both GFP and mCherry. The

western blots indicated the presence of GFP and mCherry for each dual integration strain, with different relative encapsulation levels observed for each reporter (Fig. 6A,B).

### *3.6 Encapsulation behaviors vary by cargo and cargo combination*

Results for the dual integration strains demonstrated that co-encapsulation of multiple genomic non-native cargo is feasible, and that the relative cargo encapsulation levels can be tuned using different integration locus and signal sequence combinations for each construct. However, it should be noted that the cargo encapsulation levels observed for the single integration strains may not be predictive of those for the dual integration strains, even when the same reporter construct is expressed from the same locus. This is evidenced by the western blots of purified MCPs from the dual integration strains and respective GFP and mCherry single integration strains (Fig. 6). For example, when comparing the GFP encapsulation levels for the strains LT2 *ΔpduP::ssPduP-gfpmut2* and LT2 *ΔpduP::ssPduP-gfpmut2/ΔpduD::ssPduD-mCherry* (denoted Strain IV), the encapsulation of ssPduP-GFPmut2 was lower for the dual integration strain (Fig. 6A). Conversely, when comparing the mCherry encapsulation levels for the single integration strains LT2 *ΔpduP::ssPduP-mCherry and* LT2 *ΔpduP::ssPduD(E2S)-mCherry* and the respective dual integration strains LT2 *ΔpduD::ssPduD-gfpmut2/ΔpduP::ssPduP-mCherry* (Strain I) and LT2 *ΔpduD::ssPduP-gfpmut2/ΔpduP::ssPduD(E2S)-mCherry* (Strain II), the encapsulation of the mCherry reporters was higher for both dual integration strains (Fig. 6B). The observed variations in encapsulation levels here cannot be explained by variations in expression levels, which were largely consistent between the single and dual integration strains for each reporter (Fig. 6C,D). We also noted differences in both the expression and encapsulation behaviors of GFP and mCherry reporters using the same signal sequences and integration loci for the single integration strains (Fig. 6). While some general trends can be identified, these differences show that the expression and

encapsulation levels resulting from specific integration locus and signal sequence combinations are not necessarily generalizable between the two fluorescent reporters.

The variations in encapsulation levels between single and dual integration strains may result from interactions between cargo when tagged with different signal sequences. Aggregation can occur when heterologous cargo is tagged with native Pdu signal sequences [53]. Though not directly observed for these strains, such aggregation would be expected to impact encapsulation. Previous work also explored competition between different native and non-native signal sequences for encapsulation within Pdu MCPs [32]. While this would not explain all observed variations, if such competition was occurring for different cargo combinations, it could influence their relative encapsulation levels. Regardless of mechanism, it is notable that the observed variations in encapsulation behaviors are not consistent for GFP and mCherry reporters utilizing the same integration locus and signal sequence combinations in the dual integration strains. Thus, while the overall trends observed for the genomic integration platform can be informative in selecting signal sequences and integration loci, optimization will likely be required to tune the encapsulation levels of specific heterologous cargo, including different combinations of pathway components.

## 4 Conclusions

We developed a genomic integration platform for the controllable encapsulation of heterologous cargo within Pdu MCPs. By selecting different integration locus and signal sequence combinations, we attained a range of cargo encapsulation levels, with the ability to tune the relative encapsulation levels of multiple cargo. We also demonstrated that the native Pdu signal sequences confer different encapsulation efficiencies. This will be important when selecting signal sequences for different heterologous cargo and may be of use for the design of engineered signal sequences. Efforts to expand this platform and further optimize relative encapsulation levels could include the use of such engineered signal sequences, as well as

known non-native signal sequences, *de novo* signal sequences, and any native Pdu signal sequences identified in the future.

We also determined several limitations of this genomic cargo integration platform. Specifically, we showed that not all *pdu* operon locations are permissible to cargo integrations. The expansion of this genomic integration platform to additional *pdu* operon loci would therefore require further study. Also, while the platform developed here established guidelines for selecting integration locus and signal sequence combinations to attain different encapsulation levels, optimization will likely be required when applied to other cargo and heterologous pathways. Despite these limitations, this work demonstrated the feasibility of a genomic integration platform for controllable cargo encapsulation within Pdu MCPs, and identified the key handles for tuning the encapsulation levels. Together, our results provide an additional tool for engineering Pdu MCPs towards use as tunable nanobioreactors.

## Acknowledgements

The authors would like to thank the Tullman-Ercek group, and specifically Svetlana Ikonomova, Carolyn Mills, and Han Teng Wong, for helpful comments and discussions during the preparation of this manuscript. Thanks also to Christopher Jakobson for helpful discussions for the design and construction of strains. This work was supported by the Army Research Office (grant W911NF-16-1-0169 to DTE) and the Department of Energy (grant DE-SC0019337 to DTE). TMN and NWK were supported by the National Science Foundation Graduate Research Fellowship Program (grant DGE-1842165). NWK was supported in part by the National Institutes of Health Training Grant (T32GM008449) through Northwestern University's Biotechnology Training Program. This work made use of the EPIC facility of Northwestern University's NU*ANCE* Center, which has received support from the Soft and Hybrid Nanotechnology Experimental (SHyNE) Resource (NSF ECCS-1542205); the MRSEC program

(NSF DMR-1720139) at the Materials Research Center; the International Institute for Nanotechnology (IIN); the Keck Foundation; and the State of Illinois, through the IIN.

## References


[1] R.J. Conrado, G.C. Wu, J.T. Boock, H. Xu, S.Y. Chen, T. Lebar, J. Turnšek, N. Tomšič, M. Avbelj, R. Gaber, T. Koprivnjak, J. Mori, V. Glavnik, I. Vovk, M. Benčina, V. Hodnik, G. Anderluh, J.E. Dueber, R. Jerala, M.P. DeLisa, DNA-guided assembly of biosynthetic pathways promotes improved catalytic efficiency, Nucleic Acids Research. 40 (2012) 1879–1889. https://doi.org/10.1093/nar/gkr888.

[2] C.J. Delebecque, A.B. Lindner, P.A. Silver, F.A. Aldaye, Organization of intracellular reactions with rationally designed RNA assemblies, Science. 333 (2011) 470–474.

[3] J.E. Dueber, G.C. Wu, G.R. Malmirchegini, T.S. Moon, C.J. Petzold, A.V. Ullal, K.L. Prather, J.D. Keasling, Synthetic protein scaffolds provide modular control over metabolic flux, Nature Biotechnology. 27 (2009) 753.

[4] J.H. Lee, S.-C. Jung, L.M. Bui, K.H. Kang, J.-J. Song, S.C. Kim, Improved production of L-threonine in Escherichia coli by use of a DNA scaffold system, Applied and Environmental Microbiology. 79 (2013) 774–782.

[5] J.-L. Lin, J. Zhu, I. Wheeldon, Synthetic Protein Scaffolds for Biosynthetic Pathway Colocalization on Lipid Droplet Membranes, ACS Synth. Biol. 6 (2017) 1534–1544. https://doi.org/10.1021/acssynbio.7b00041.

[6] T.S. Moon, J.E. Dueber, E. Shiue, K.L.J. Prather, Use of modular, synthetic scaffolds for improved production of glucaric acid in engineered E. coli, Metabolic Engineering. 12 (2010) 298–305.

[7] G. Sachdeva, A. Garg, D. Godding, J.C. Way, P.A. Silver, In vivo co-localization of enzymes on RNA scaffolds increases metabolic production in a geometrically dependent manner, Nucleic Acids Research. 42 (2014) 9493–9503.

[8] R.J. Conrado, T.J. Mansell, J.D. Varner, M.P. DeLisa, Stochastic reaction–diffusion simulation of enzyme compartmentalization reveals improved catalytic efficiency for a synthetic metabolic pathway, Metabolic Engineering. 9 (2007) 355–363. https://doi.org/10.1016/j.ymben.2007.05.002.

[9] C.M. Jakobson, D. Tullman-Ercek, N.M. Mangan, Spatially organizing biochemistry: choosing a strategy to translate synthetic biology to the factory, Scientific Reports. 8 (2018) 8196. https://doi.org/10.1038/s41598-018-26399-0.

[10] F. Hinzpeter, U. Gerland, F. Tostevin, Optimal compartmentalization strategies for metabolic microcompartments, Biophysical Journal. 112 (2017) 767–779.

[11] C.A. Kerfeld, C. Aussignargues, J. Zarzycki, F. Cai, M. Sutter, Bacterial microcompartments, Nature Reviews Microbiology. 16 (2018) 277–290. https://doi.org/10.1038/nrmicro.2018.10.

[12] S.D. Axen, O. Erbilgin, C.A. Kerfeld, A taxonomy of bacterial microcompartment loci constructed by a novel scoring method, PLoS Computational Biology. 10 (2014) e1003898.

[13] T.A. Bobik, G.D. Havemann, R.J. Busch, D.S. Williams, H.C. Aldrich, The Propanediol Utilization (pdu) Operon ofSalmonella enterica Serovar Typhimurium LT2 Includes Genes Necessary for Formation of Polyhedral Organelles Involved in Coenzyme B12-Dependent 1, 2-Propanediol Degradation, Journal of Bacteriology. 181 (1999) 5967–5975.

[14] T.A. Bobik, Y. Xu, R.M. Jeter, K.E. Otto, J.R. Roth, Propanediol utilization genes (pdu) of Salmonella typhimurium: three genes for the propanediol dehydratase, Journal of Bacteriology. 179 (1997) 6633–6639.

[15] A.R. Horswill, J.C. Escalante-Semerena, Salmonella typhimurium LT2 catabolizes propionate via the 2-methylcitric acid cycle, Journal of Bacteriology. 181 (1999) 5615–5623.

[16] N.A. Leal, G.D. Havemann, T.A. Bobik, PduP is a coenzyme-a-acylating propionaldehyde dehydrogenase associated with the polyhedral bodies involved in B12-dependent 1, 2-propanediol degradation by Salmonella enterica serovar Typhimurium LT2, Archives of Microbiology. 180 (2003) 353–361.

[17] Y. Liu, N.A. Leal, E.M. Sampson, C.L. Johnson, G.D. Havemann, T.A. Bobik, PduL is an evolutionarily distinct phosphotransacylase involved in B12-dependent 1, 2-propanediol degradation by Salmonella enterica serovar Typhimurium LT2, Journal of Bacteriology. 189 (2007) 1589–1596.
[18] S. Palacios, V.J. Starai, J.C. Escalante-Semerena, Propionyl coenzyme A is a common intermediate in the 1, 2-propanediol and propionate catabolic pathways needed for expression of the prpBCDE operon during growth of Salmonella enterica on 1, 2-propanediol, Journal of Bacteriology. 185 (2003) 2802–2810.
[19] E.M. Sampson, T.A. Bobik, Microcompartments for B12-dependent 1, 2-propanediol degradation provide protection from DNA and cellular damage by a reactive metabolic intermediate, Journal of Bacteriology. 190 (2008) 2966–2971.
[20] C. Chowdhury, S. Chun, A. Pang, M.R. Sawaya, S. Sinha, T.O. Yeates, T.A. Bobik, Selective molecular transport through the protein shell of a bacterial microcompartment organelle, Proceedings of the National Academy of Sciences of the United States of America. 112 (2015) 2990–2995. https://doi.org/10.1073/pnas.1423672112.
[21] C.S. Crowley, D. Cascio, M.R. Sawaya, J.S. Kopstein, T.A. Bobik, T.O. Yeates, Structural insight into the mechanisms of transport across the Salmonella enterica Pdu microcompartment shell, Journal of Biological Chemistry. 285 (2010) 37838–37846.
[22] G.D. Havemann, E.M. Sampson, T.A. Bobik, PduA is a shell protein of polyhedral organelles involved in coenzyme B12-dependent degradation of 1, 2-propanediol in Salmonella enterica serovar Typhimurium LT2, Journal of Bacteriology. 184 (2002) 1253–1261.
[23] C.M. Jakobson, D. Tullman-Ercek, M.F. Slininger, N.M. Mangan, A systems-level model reveals that 1, 2-Propanediol utilization microcompartments enhance pathway flux through intermediate sequestration, PLoS Computational Biology. 13 (2017) e1005525.
[24] S. Cheng, C. Fan, S. Sinha, T.A. Bobik, The PduQ enzyme is an alcohol dehydrogenase used to recycle NAD+ internally within the Pdu microcompartment of Salmonella enterica, PLoS One. 7 (2012) e47144.
[25] Y. Liu, J. Jorda, T.O. Yeates, T.A. Bobik, The PduL phosphotransacylase is used to recycle coenzyme A within the Pdu microcompartment, Journal of Bacteriology. 197 (2015) 2392–2399.
[26] S. Cheng, T.A. Bobik, Characterization of the PduS cobalamin reductase of Salmonella enterica and its role in the Pdu microcompartment, Journal of Bacteriology. 192 (2010) 5071–5080.
[27] H.J. Wagner, C.C. Capitain, K. Richter, M. Nessling, J. Mampel, Engineering bacterial microcompartments with heterologous enzyme cargos, Engineering in Life Sciences. 17 (2017) 36–46.
[28] A.D. Lawrence, S. Frank, S. Newnham, M.J. Lee, I.R. Brown, W.-F. Xue, M.L. Rowe, D.P. Mulvihill, M.B. Prentice, M.J. Howard, Solution structure of a bacterial microcompartment targeting peptide and its application in the construction of an ethanol bioreactor, ACS Synthetic Biology. 3 (2014) 454–465.
[29] C.M. Jakobson, Y. Chen, M.F. Slininger, E. Valdivia, E.Y. Kim, D. Tullman-Ercek, Tuning the Catalytic Activity of Subcellular Nanoreactors, Journal of Molecular Biology. 428 (2016) 2989–2996.
[30] C. Fan, S. Cheng, Y. Liu, C.M. Escobar, C.S. Crowley, R.E. Jefferson, T.O. Yeates, T.A. Bobik, Short N-terminal sequences package proteins into bacterial microcompartments, Proceedings of the National Academy of Sciences of the United States of America. 107 (2010) 7509–14. https://doi.org/10.1073/pnas.0913199107.
[31] C. Fan, T.A. Bobik, The N-terminal region of the medium subunit (PduD) packages adenosylcobalamin-dependent diol dehydratase (PduCDE) into the Pdu microcompartment, Journal of Bacteriology. 193 (2011) 5623–5628.

[32] C.M. Jakobson, E.Y. Kim, M.F. Slininger, A. Chien, D. Tullman-Ercek, Localization of Proteins to the 1, 2-Propanediol Utilization Microcompartment by Non-native Signal Sequences Is Mediated by a Common Hydrophobic Motif, Journal of Biological Chemistry. 290 (2015) 24519–24533.
[33] C.M. Jakobson, M.F. Slininger Lee, D. Tullman-Ercek, De novo design of signal sequences to localize cargo to the 1, 2-propanediol utilization microcompartment, Protein Science. 26 (2017) 1086–1092.
[34] M.J. Lee, J. Mantell, I.R. Brown, J.M. Fletcher, P. Verkade, R.W. Pickersgill, D.N. Woolfson, S. Frank, M.J. Warren, De novo targeting to the cytoplasmic and luminal side of bacterial microcompartments, Nature Communications. 9 (2018) 3413. https://doi.org/10.1038/s41467-018-05922-x.
[35] S. Oesterle, I. Wuethrich, S. Panke, Toward Genome-Based Metabolic Engineering in Bacteria, in: Advances in Applied Microbiology, Elsevier, 2017: pp. 49–82.
[36] J.A. Englaender, J.A. Jones, B.F. Cress, T.E. Kuhlman, R.J. Linhardt, M.A. Koffas, Effect of genomic integration location on heterologous protein expression and metabolic engineering in E. coli, ACS Synthetic Biology. 6 (2017) 710–720.
[37] M.C. Bassalo, A.D. Garst, A.L. Halweg-Edwards, W.C. Grau, D.W. Domaille, V.K. Mutalik, A.P. Arkin, R.T. Gill, Rapid and efficient one-step metabolic pathway integration in E. coli, ACS Synthetic Biology. 5 (2016) 561–568.
[38] T.A. Bobik, M. Ailion, J.R. Roth, A single regulatory gene integrates control of vitamin B12 synthesis and propanediol degradation, Journal of Bacteriology. 174 (1992) 2253–2266.
[39] M.R. Rondon, J.C. Escalante-Semerena, The poc locus is required for 1, 2-propanediol-dependent transcription of the cobalamin biosynthetic (cob) and propanediol utilization (pdu) genes of Salmonella typhimurium, Journal of Bacteriology. 174 (1992) 2267–2272.
[40] M.R. Rondon, J.C. Escalante-Semerena, In vitro analysis of the interactions between the PocR regulatory protein and the promoter region of the cobalamin biosynthetic (cob) operon of Salmonella typhimurium LT2, Journal of Bacteriology. 178 (1996) 2196–2203.
[41] S. Datta, N. Costantino, D.L. Court, A set of recombineering plasmids for gram-negative bacteria, Gene. 379 (2006) 109–115.
[42] L. Thomason, D.L. Court, M. Bubunenko, N. Costantino, H. Wilson, S. Datta, A. Oppenheim, Recombineering: Genetic Engineering in Bacteria Using Homologous Recombination, in: Current Protocols in Molecular Biology, John Wiley & Sons, Inc., 2001. http://onlinelibrary.wiley.com/doi/10.1002/0471142727.mb0116s78/abstract (accessed June 13, 2013).
[43] E.Y. Kim, D. Tullman-Ercek, A rapid flow cytometry assay for the relative quantification of protein encapsulation into bacterial microcompartments, Biotechnology Journal. 9 (2014) 348–354.
[44] B.P. Cormack, R.H. Valdivia, S. Falkow, FACS-optimized mutants of the green fluorescent protein (GFP), Gene. 173 (1996) 33–38.
[45] N.C. Shaner, R.E. Campbell, P.A. Steinbach, B.N. Giepmans, A.E. Palmer, R.Y. Tsien, Improved monomeric red, orange and yellow fluorescent proteins derived from Discosoma sp. red fluorescent protein, Nature Biotechnology. 22 (2004) 1567.
[46] T.M. Nichols, N.W. Kennedy, D. Tullman-Ercek, Cargo encapsulation in bacterial microcompartments: Methods and analysis, in: C. Schmidt-Dannert, M.B. Quin (Eds.), Methods in Enzymology, Academic Press, 2019: pp. 155–186. https://doi.org/10.1016/bs.mie.2018.12.009.
[47] C. Engler, R. Gruetzner, R. Kandzia, S. Marillonnet, Golden Gate Shuffling: A One-Pot DNA Shuffling Method Based on Type IIs Restriction Enzymes, PLoS ONE. 4 (2009) e5553. https://doi.org/10.1371/journal.pone.0005553.

[48] S. Sinha, S. Cheng, C. Fan, T.A. Bobik, The PduM protein is a structural component of the microcompartments involved in coenzyme B12-dependent 1, 2-propanediol degradation by Salmonella enterica, Journal of Bacteriology. 194 (2012) 1912–1918.
[49] C.A. Schneider, W.S. Rasband, K.W. Eliceiri, NIH Image to ImageJ: 25 years of image analysis, Nat Meth. 9 (2012) 671–675. https://doi.org/10.1038/nmeth.2089.
[50] C.M. Farrell, A.D. Grossman, R.T. Sauer, Cytoplasmic degradation of ssrA-tagged proteins, Molecular Microbiology. 57 (2005) 1750–1761. https://doi.org/10.1111/j.1365-2958.2005.04798.x.
[51] S. Gottesman, E. Roche, Y. Zhou, R.T. Sauer, The ClpXP and ClpAP proteases degrade proteins with carboxy-terminal peptide tails added by the SsrA-tagging system, Genes & Development. 12 (1998) 1338–1347.
[52] S. Cheng, S. Sinha, C. Fan, Y. Liu, T.A. Bobik, Genetic analysis of the protein shell of the microcompartments involved in coenzyme B12-dependent 1, 2-propanediol degradation by Salmonella, Journal of Bacteriology. 193 (2011) 1385–1392.
[53] M.J. Lee, I.R. Brown, R. Juodeikis, S. Frank, M.J. Warren, Employing bacterial microcompartment technology to engineer a shell-free enzyme-aggregate for enhanced 1,2-propanediol production in Escherichia coli, Metabolic Engineering. 36 (2016) 48–56. https://doi.org/10.1016/j.ymben.2016.02.007.

## Figure Captions

**Fig. 1. Modifying the Pdu MCP and *pdu* operon for heterologous cargo encapsulation. (A)** Diagram of the native pathway for 1,2-PD metabolism within the Pdu MCP (left; adapted from Methods in Enzymology, Vol. 617, T.M. Nichols, N.W. Kennedy, D. Tullman-Ercek, Cargo encapsulation in bacterial microcompartments: Methods and analysis, pp. 155–186, Academic Press (2019), with permission from Elsevier). The Pdu MCP shell (hexagon) encapsulates the Pdu enzymes as well as the substrates and cofactors required for the pathway. Engineering the native Pdu MCP would enable the use of this structure as an enclosed scaffold for the compartmentalization of heterologous pathways (right). **(B)** Diagram of the genomic cargo integration platform developed in *S. enterica* LT2. Different fluorescent reporters, including GFP tagged with Pdu signal sequences and untagged GFP, were individually integrated into the *pdu* operon in place of the native Pdu enzymes PduD, PduL, PduP, or PduQ.

**Fig. 2. Encapsulation levels vary for GFP reporters expressed from the *pduD* locus. (A)** Phase contrast and GFP fluorescence microscopy of the *pduD* locus integration strains and wild-type *S. enterica* LT2 (LT2 WT), with transmission electron micrographs (TEM) of purified MCPs. Column labels indicate the source strain for the images shown; the *pduD* locus integration strains are denoted by the signal sequence used for the integrated GFP reporter. White scale bars represent 1 μm and black scale bars represent 200 nm. **(B)** Coomassie stained SDS-PAGE of purified MCPs (top) and αGFP western blots of purified MCPs (MCP) and whole cell lysate (WCL) samples (bottom) from the *pduD* locus integration strains (denoted as above), LT2 WT, and the non-assembly control *S. enterica* LT2 *ΔpocR* (ΔpocR). Lane labels indicate the source strain. Detection of GFP for MCP samples indicates encapsulation and detection of GFP for WCL samples indicates expression, with band intensities indicating the relative levels. **(C)** Relative encapsulation levels for the *pduD* locus integration strains (denoted as above), determined by densitometry analysis of MCP western blots. Values are shown

relative to the encapsulation level for LT2 *ΔpduD::ssPduP-gfpmut2*, which was present on all western blots analyzed. The value reported for each strain is the average relative encapsulation ratio calculated from western blots of MCPs from three separate purifications. Error bars indicate standard error. Statistical significance for comparisons with LT2 *ΔpduD::ssPduP-gfpmut2* determined by one-sample t-tests (for mean=1). Statistical significance otherwise determined by two-sample, one-tailed t-tests for comparisons shown. Significance of $p<0.05$ is indicated by *, while N.S. is $p>0.10$. Note there was also no statistically significant difference between LT2 *ΔpduD::ssPduL-gfpmut2* and LT2 *ΔpduD::gfpmut2* as determined by a two-sample, two-tailed t-test. **(D)** Relative expression levels for the *pduD* locus integration strains (denoted as above), determined by densitometry analysis of WCL western blots. Values are shown relative to the expression level of LT2 *ΔpduD::ssPduP-gfpmut2*, which was present on all western blots analyzed. The value reported for each strain is the average relative expression ratio calculated from western blots of WCL prepared from culture samples reserved prior to harvest for the purifications in (C). Error bars indicate standard error. No statistically significant differences were found for the relative expression levels (single factor ANOVA, $p=0.120$).

**Fig. 3. Relative encapsulation and expression levels for the *pduL*, *pduP*, and *pduQ* locus integration strains.** Bar graph labels denote source strains by the integration locus and signal sequence used for the GFP reporter. **(A)** Relative encapsulation levels for the *pduL* (green), *pduP* (blue), and *pduQ* (pink) locus integration strains, determined by densitometry analysis of MCP western blots. Values are shown relative to the encapsulation level for LT2 *ΔpduD::ssPduP-gfpmut2* (orange), which was present on all western blots analyzed. The value reported for each strain is the average relative encapsulation ratio calculated from western blots of MCPs from three separate purifications. Error bars indicate standard error. Statistical significance determined by two-sample, one-tailed t-tests unless noted below. Significance of $p<0.05$ is indicated by * and of $p<0.10$ is indicated by **. For the comparison between

*ΔpduP::ssPduD(E2S)-gfpmut2* and *ΔpduP::ssPduP-gfpmut2*, N.S. is p>0.10 as determined by a two-sample, two-tailed t-test. Note there was also no statistically significant difference between ssPduL and No Tag for either the *pduL* or p*duQ* locus strains as determined by two-sample, two-tailed t-tests. **(B)** Relative expression levels for the *pduL* (green/grey), *pduP* (blue/grey), and *pduQ* (pink/grey) locus integration strains, determined by densitometry analysis of WCL western blots. Values are shown relative to the expression level of LT2 *ΔpduD::ssPduP-gfpmut2* (orange/grey), which was present on all western blots analyzed. The value reported for each strain is the average relative expression ratio calculated from western blots of WCL prepared from culture samples reserved prior to harvest for the purifications in (A). Error bars indicate standard error. No statistically significant differences were found for the relative cargo expression levels for the *pduL* locus integration strains (single factor ANOVA, p=0.867), *pduP* locus integration strains (single factor ANOVA, p=0.221), or the *pduQ* locus integration strains (single factor ANOVA, p=0.667).

**Fig. 4. Integrations at the pduL locus result in aberrant cell and MCP phenotypes.** Phase contrast and GFP fluorescence microscopy of the *pduL* locus integration strains and LT2 WT, with TEM of purified MCPs/protein structures. Column labels indicate the source strain for the images shown; the *pduL* locus integration strains are denoted by the signal sequence used for the integrated GFP reporter. White scale bars represent 1 μm and black scale bars represent 200 nm.

**Fig. 5. Dual integration strains demonstrate co-encapsulation of multiple genomically encoded cargo within Pdu MCPs.** **(A)** Diagram of the *S. enterica* LT2 dual integration strains, denoted as Strains I-IV. For each strain, a tagged GFP reporter and a tagged mCherry reporter were each integrated at either the *pduD* or *pduP* locus. Note that ssPduD* indicates the use of ssPduD or ssPduD(E2S) depending on the integration locus: Strain I: LT2 *ΔpduD::ssPduD-gfpmut2/ΔpduP::ssPduP-mCherry,* Strain II: LT2 *ΔpduD::ssPduP-*

*gfpmut2/ΔpduP::ssPduD(E2S)-mCherry*, Strain III: LT2 *ΔpduP::ssPduD(E2S)-gfpmut2/ΔpduD::ssPduP-mCherry,* Strain IV: LT2 *ΔpduP::ssPduP-gfpmut2/ΔpduD::ssPduD-mCherry.* **(B)** Phase contrast, GFP fluorescence, and mCherry fluorescence microscopy of *S. enterica* LT2 dual integration strains and LT2 WT, with TEM of purified MCPs. Column labels indicate the source strain for the images shown. The GFP fluorescence images and mCherry fluorescence images were adjusted to more clearly show the observed fluorescent puncta; the images in each panel were therefore not adjusted identically. White scale bars represent 1 μm and black scale bars represent 200 nm.

**Fig. 6. Co-encapsulation of multiple genomically encoded cargo can be attained with varying relative encapsulation levels.** Coomassie stained SDS-PAGE of purified MCPs (top) and **(A)** αGFP western blots of purified MCPs, **(B)** αmCherry western blots of purified MCPs, **(C)** αGFP western blots of WCL samples, and **(D)** αmCherry western blots of WCL samples from GFP single integration strains (“GFP Only” lanes), dual integration strains (“GFP and mCherry” lanes), and mCherry single integration strains (“mCherry Only” lanes), LT2 WT, and LT2 *ΔpocR*. Lane labels indicate the source strain, where GFP and mCherry single integration strains are denoted by the integration locus and signal sequence used for the respective reporter, and dual integration strains are denoted as follows: Strain I: LT2 *ΔpduD::ssPduD-gfpmut2/ΔpduP::ssPduP-mCherry,* Strain II: LT2 *ΔpduD::ssPduP-gfpmut2/ΔpduP::ssPduD(E2S)-mCherry*, Strain III: LT2 *ΔpduP::ssPduD(E2S)-gfpmut2/ΔpduD::ssPduP-mCherry,* Strain IV: LT2 *ΔpduP::ssPduP-gfpmut2/ΔpduD::ssPduD-mCherry.* Detection of (A) GFP or (B) mCherry for MCP samples indicates encapsulation and detection of (C) GFP or (D) mCherry for WCL samples indicates expression, with band intensities indicating the relative levels.

## Figures and Tables

**Figure 1** – Color in print

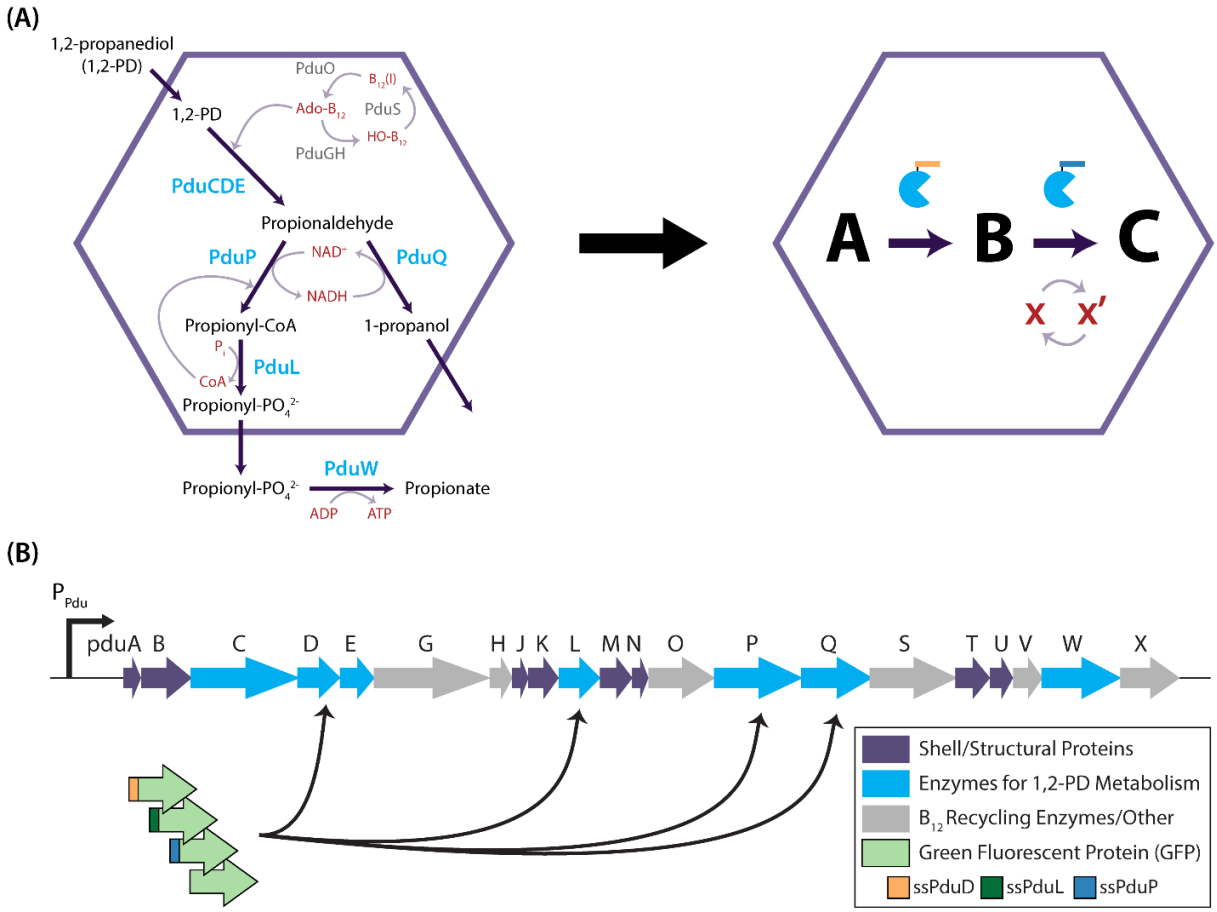

**Figure 2** - Color in print

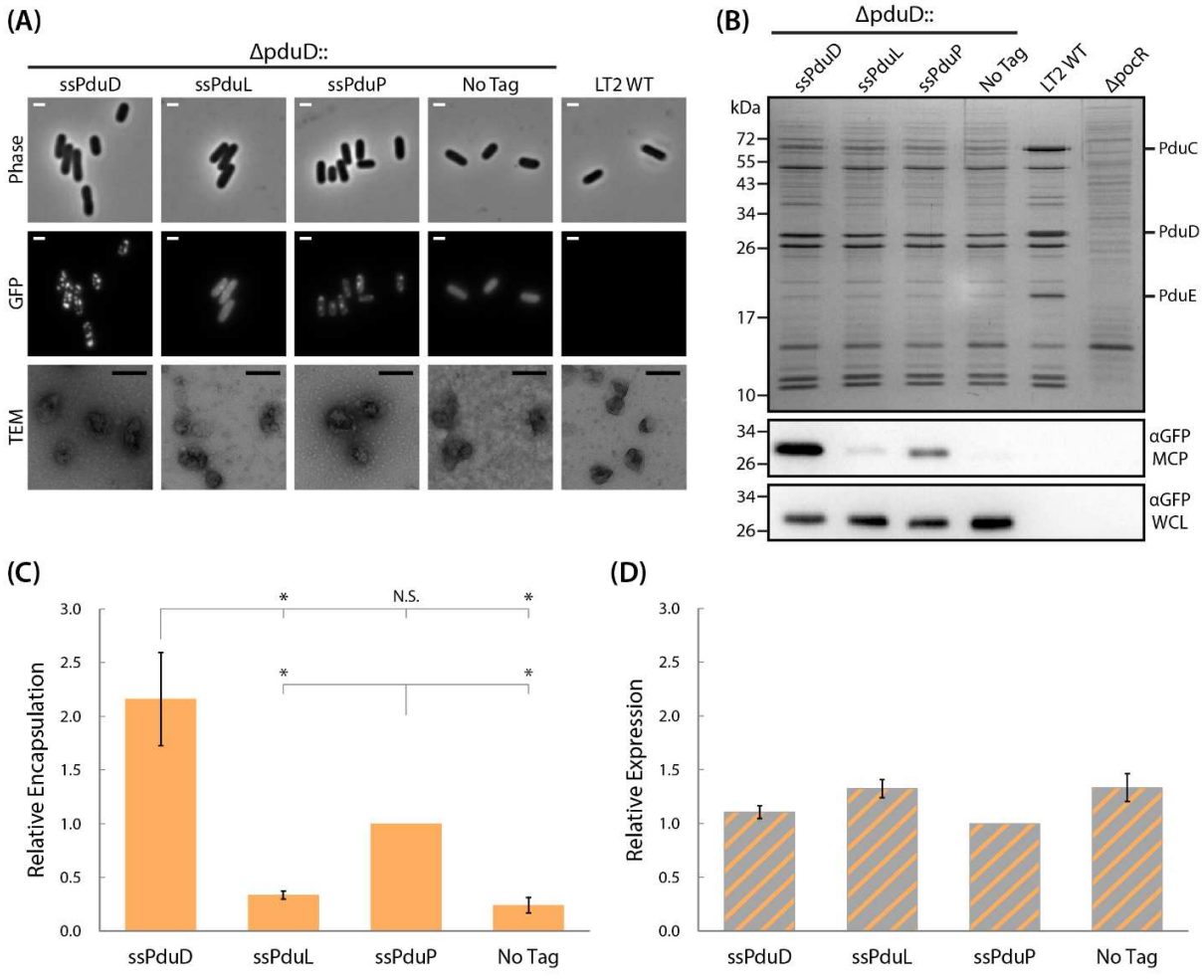

**Figure 3** – Color in print

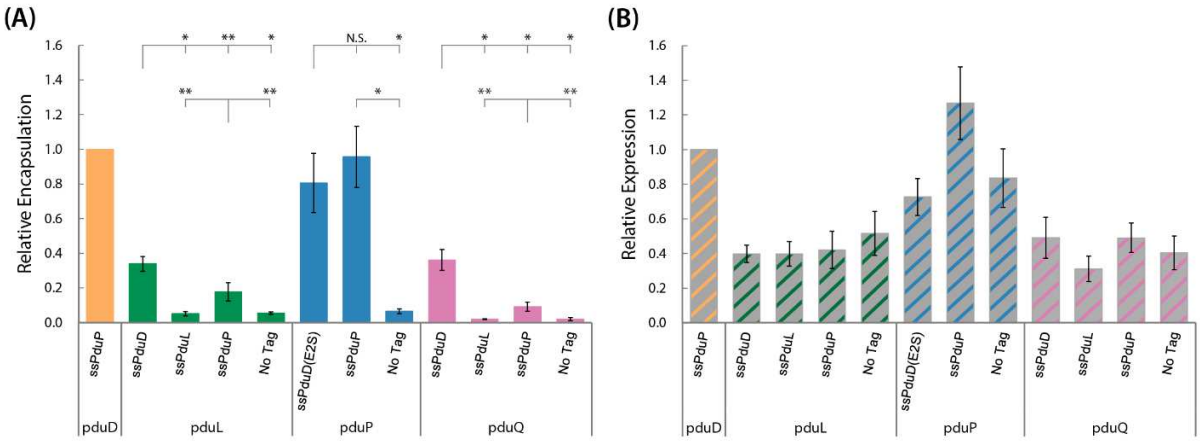

**Figure 4**

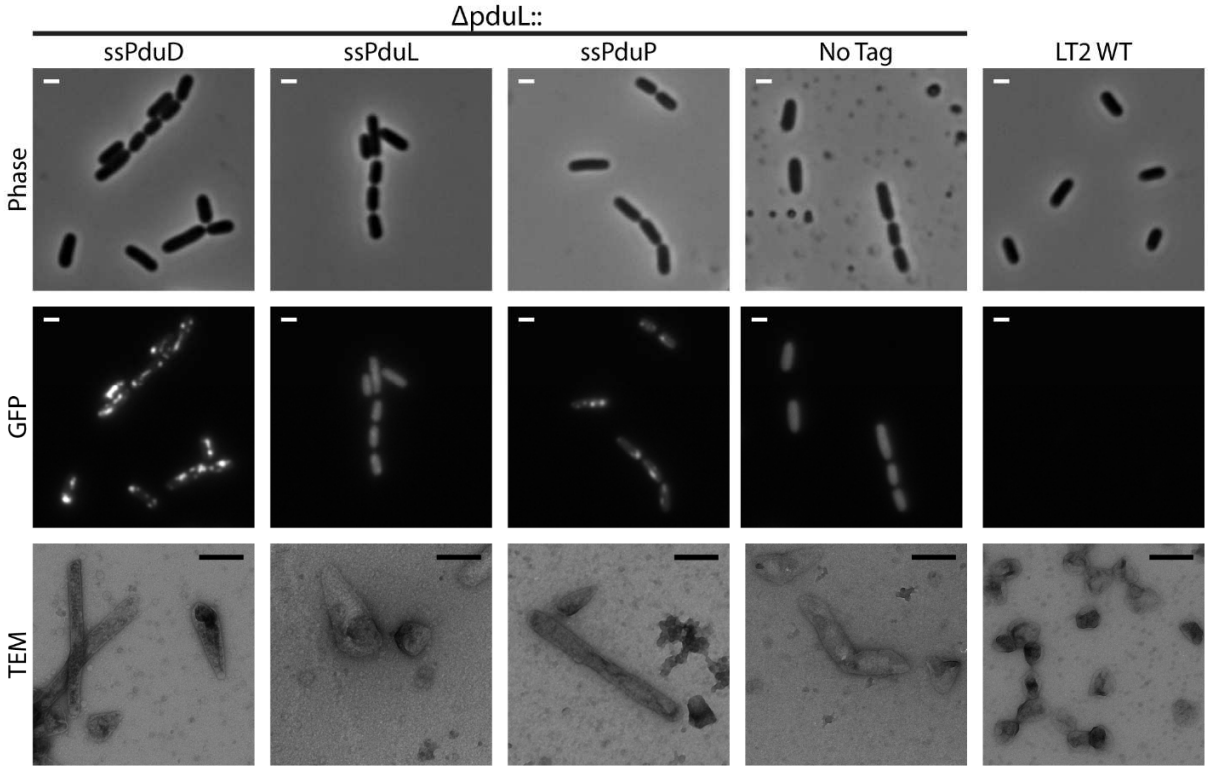

**Figure 5** – Color in print

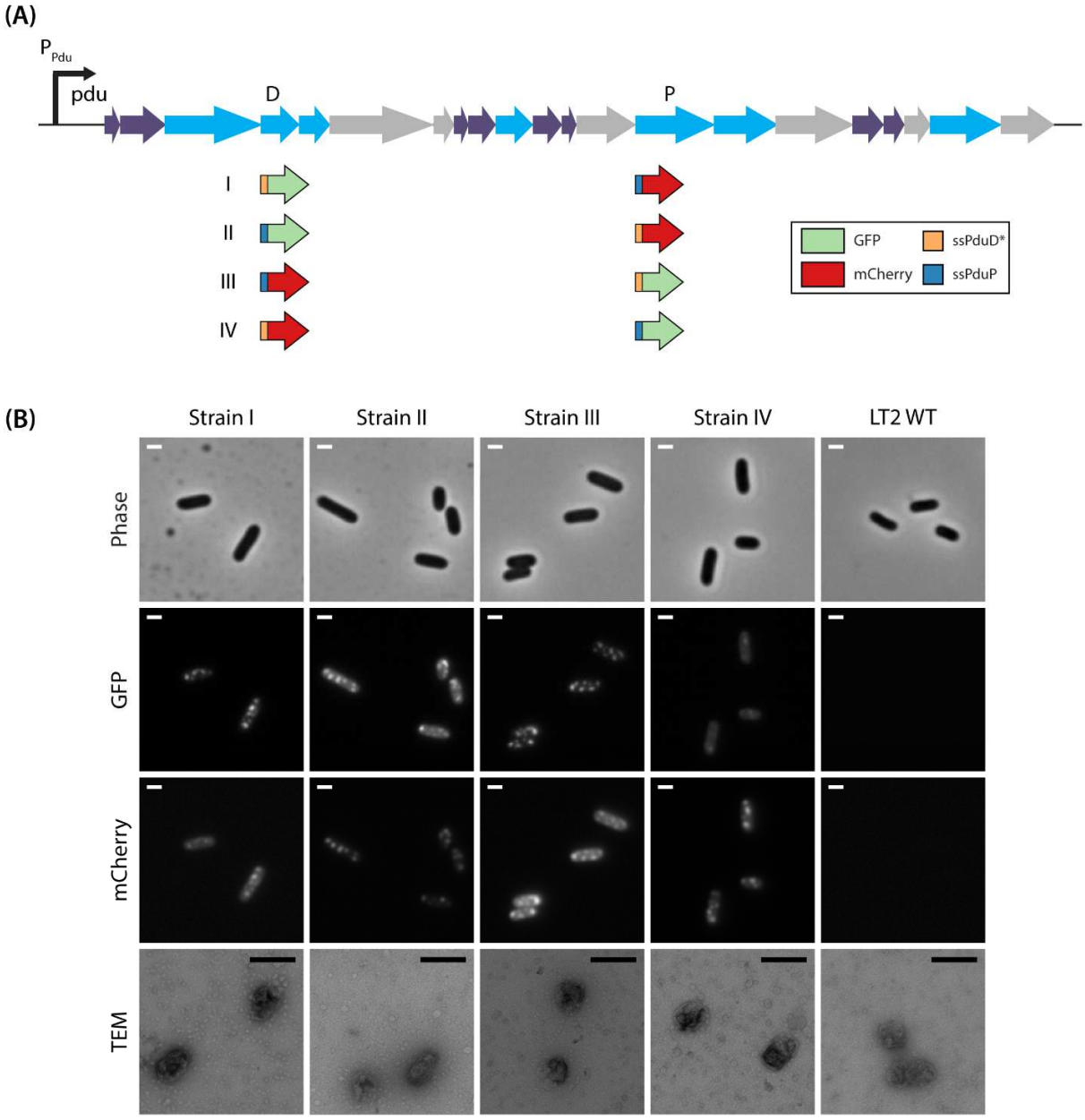

**Figure 6**

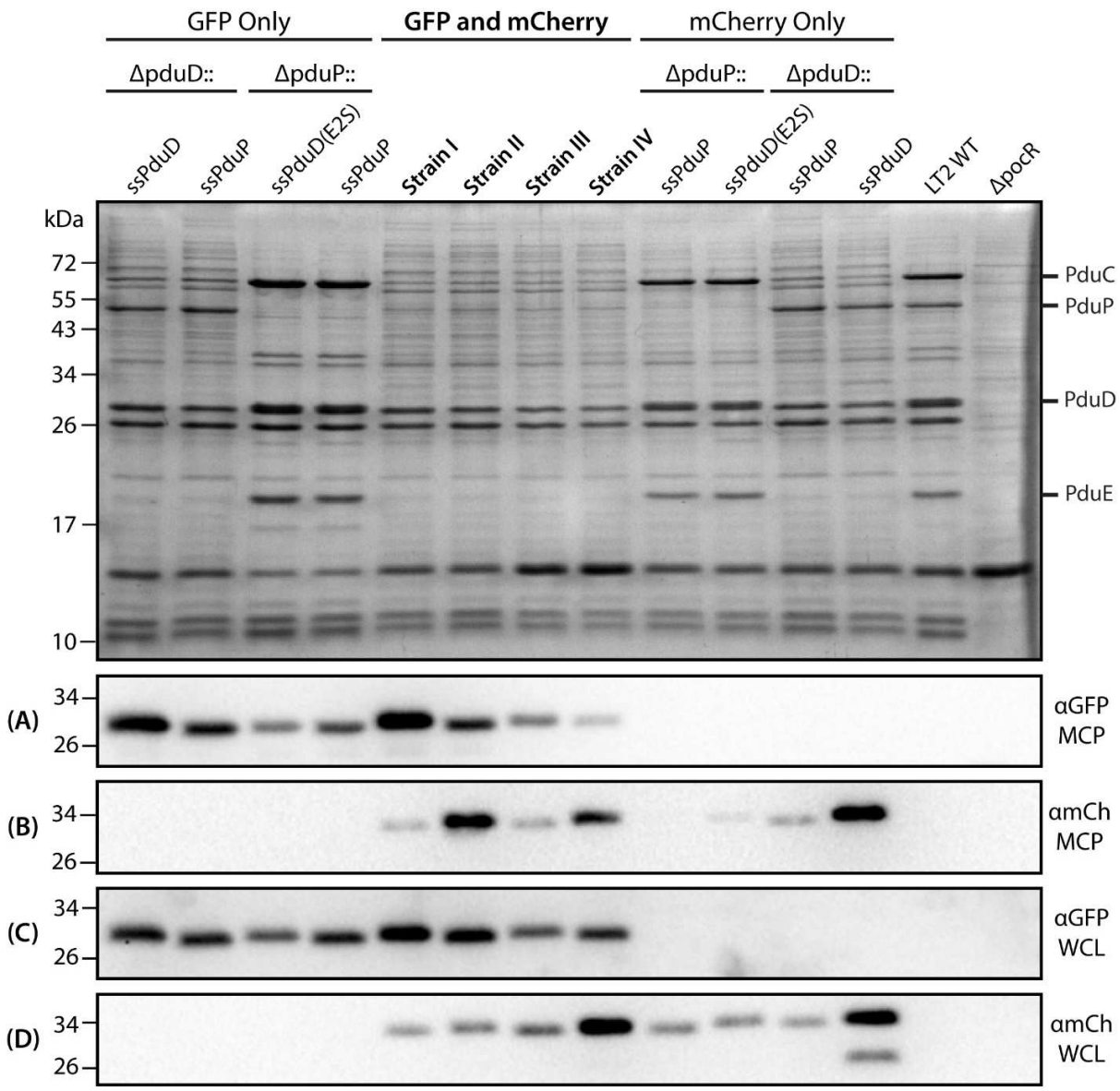
GFP Only
GFP and mCherry
mCherry Only
ΔpduD::
ΔpduP::
ΔpduP::
ΔpduD::
ssPduD
ssPduP
ssPduD(E2S)
ssPduP
Strain I
Strain II
Strain III
Strain IV
ssPduP
ssPduD(E2S)
ssPduP
ssPduD
LT2 WT
ΔpocR
kDa
72
55
43
34
26
17
10
PduC
PduP
PduD
PduE
(A)
34
26
αGFP MCP
(B)
34
26
αmCh MCP
(C)
34
26
αGFP WCL
(D)
34
26
αmCh WCL

**Table 1:** Bacterial strains used in this study

| Strain | Organism | Genotype |
|---|---|---|
| EYKS003 | *E. coli* | DH10B wild type |
| TUC01 [41,42] | *E. coli* | *cat/sacB* |
| TMDS004 | *S. enterica* serovar Typhimurium | LT2 wild type |
| TMDS011 | *S. enterica* serovar Typhimurium | LT2 *ΔpocR* |
| TMDS031 | *S. enterica* serovar Typhimurium | LT2 *ΔpduD::cat/sacB* |
| TMDS025 | *S. enterica* serovar Typhimurium | LT2 *ΔpduD::ssPduD-gfpmut2* |
| TMDS078 | *S. enterica* serovar Typhimurium | LT2 *ΔpduD::ssPduL-gfpmut2* |
| TMDS027 | *S. enterica* serovar Typhimurium | LT2 *ΔpduD::ssPduP-gfpmut2* |
| TMDS029 | *S. enterica* serovar Typhimurium | LT2 *ΔpduD::gfpmut2* |
| TMDS068 | *S. enterica* serovar Typhimurium | LT2 *ΔpduL::cat/sacB* |
| TMDS085 | *S. enterica* serovar Typhimurium | LT2 *ΔpduL::ssPduD-gfpmut2* |
| TMDS086 | *S. enterica* serovar Typhimurium | LT2 *ΔpduL::ssPduL-gfpmut2* |
| TMDS087 | *S. enterica* serovar Typhimurium | LT2 *ΔpduL::ssPduP-gfpmut2* |
| TMDS088 | *S. enterica* serovar Typhimurium | LT2 *ΔpduL::gfpmut2* |
| CMJS374 [32] | *S. enterica* serovar Typhimurium | LT2 *ΔpduP::cat/sacB* |
| TMDS089 | *S. enterica* serovar Typhimurium | LT2 *ΔpduP::ssPduD(E2S)-gfpmut2* |
| TMDS021 | *S. enterica* serovar Typhimurium | LT2 *ΔpduP::ssPduP-gfpmut2* |
| TMDS023 | *S. enterica* serovar Typhimurium | LT2 *ΔpduP::gfpmut2* |
| TMDS069 | *S. enterica* serovar Typhimurium | LT2 *ΔpduQ::cat/sacB* |
| TMDS091 | *S. enterica* serovar Typhimurium | LT2 *ΔpduQ::ssPduD-gfpmut2* |
| TMDS092 | *S. enterica* serovar Typhimurium | LT2 *ΔpduQ::ssPduL-gfpmut2* |
| TMDS093 | *S. enterica* serovar Typhimurium | LT2 *ΔpduQ::ssPduP-gfpmut2* |
| TMDS094 | *S. enterica* serovar Typhimurium | LT2 *ΔpduQ::gfpmut2* |
| TMDS107 | *S. enterica* serovar Typhimurium | LT2 *ΔpduD::ssPduD-mCherry* |
| TMDS108 | *S. enterica* serovar Typhimurium | LT2 *ΔpduD::ssPduP-mCherry* |
| TMDS109 | *S. enterica* serovar Typhimurium | LT2 *ΔpduP::ssPduD(E2S)-mCherry* |
| TMDS110 | *S. enterica* serovar Typhimurium | LT2 *ΔpduP::ssPduP-mCherry* |
| TMDS099 | *S. enterica* serovar Typhimurium | LT2 *ΔpduD::ssPduD-gfpmut2/ ΔpduP::cat/sacB* |
| TMDS100 | *S. enterica* serovar Typhimurium | LT2 *ΔpduD::ssPduP-gfpmut2/ ΔpduP::cat/sacB* |
| TMDS101 | *S. enterica* serovar Typhimurium | LT2 *ΔpduP::ssPduD(E2S)-gfpmut2/ ΔpduD::cat/sacB* |
| TMDS102 | *S. enterica* serovar Typhimurium | LT2 *ΔpduP::ssPduP-gfpmut2/ ΔpduD::cat/sacB* |
| TMDS111 | *S. enterica* serovar Typhimurium | LT2 *ΔpduD::ssPduD-gfpmut2/ ΔpduP::ssPduP-mCherry* |
| TMDS112 | *S. enterica* serovar Typhimurium | LT2 *ΔpduD::ssPduP-gfpmut2/ ΔpduP::ssPduD(E2S)-mCherry* |
| TMDS113 | *S. enterica* serovar Typhimurium | LT2 *ΔpduP::ssPduD(E2S)-gfpmut2/ ΔpduD::ssPduP-mCherry* |
| TMDS114 | *S. enterica* serovar Typhimurium | LT2 *ΔpduP::ssPduP-gfpmut2/ ΔpduD::ssPduD-mCherry* |

**Table 2:** Plasmids used in this study

| Plasmid | Genotype | Antibiotic Resistance |
|---|---|---|
| pSIM6 [41] | λ-red | Carbenicillin |
| EYK250 | pBAD33t Golden Gate sfGFP | Chloramphenicol |
| EYK252 | BBpTET pSC101 Golden Gate sfGFP | Kanamycin |
| CMJ038 [32] | pBAD *ssPduD-gfpmut2-ssrA* | Chloramphenicol |
| TMD010 | pBAD *ssPduD(E2S)-gfpmut2-ssrA* | Chloramphenicol |
| TMD005 | pBAD *ssPduL-gfpmut2-ssrA* | Chloramphenicol |
| TMD011 | pBAD *ssPduL(D2S)-gfpmut2-ssrA* | Chloramphenicol |
| EYK054 [43] | pBAD *ssPduP-gfpmut2-ssrA* | Chloramphenicol |
| CMJ206 [32] | pTET *ssPduD-mCherry-ssrA* | Kanamycin |
| TMD012 | pTET *ssPduD(E2S)-mCherry-ssrA* | Kanamycin |
| CMJ205 [32] | pTET *ssPduP-mCherry-ssrA* | Kanamycin |
| TMD006 | pBAD *ssPduD-gfpmut2-ssrA(AAV)* | Chloramphenicol |
| TMD008 | pBAD *ssPduP-gfpmut2-ssrA(AAV)* | Chloramphenicol |